Mateo-Mateo, D.; Asiri, AM.; Albero-Sancho, J.; García Gómez, H. (2018). The mechanism of photocatalytic CO2 reduction by graphene-supported Cu2O probed by sacrificial electron donors. Photochemical & Photobiological Sciences. 17(6):829-834. https://doi.org/10.1039/c7pp00442g

Journal Name

ARTICLE

The mechanism of the photocatalytic CO_2 reduction by graphene supported Cu_2O probed by sacrificial electron donors

Received 00th January 20xx,
Accepted 00th January 20xx

DOI: 10.1039/x0xx00000x

www.rsc.org/

Diego Mateo,[a] Abdullah M. Asiri,[b] Josep Albero*,[a] and Hermenegildo García[a,b]

Cu_2O nanoparticles of 5 nm average size have been adsorbed at 1.74 wt. % on defective graphene (Cu_2O/G) previously obtained by pyrolysis of alginic acid. The Cu_2O crystal phase determined by XRD. XPS shows that the external layers of the Cu_2O nanoparticles are constituted mainly by Cu^{+} although a certain percentage of Cu^{+II} was also present. Cu_2O/G is a photocatalyst for the CO_2 reduction to methane in the presence of sacrificial agents, the rate of CH_4 production depending on the oxidation potential of the electron donor. This relationship supports a mechanism involving photoinduced charge separation with the generation of electrons and holes. The highest CH_4 formation rate upon UV-Vis irradiation of Cu_2O/G with a 300 W Xe lamp was achieved for dimethylaniline reaching 326 μmol $CH_4 \cdot g^{-1} \cdot h^{-1}$. The spectral response of the Cu_2O photocatalyst shows, however, that the response of the photocatalyst is mainly due to UV irradiation, indicating that light absorption at the low Cu_2O loading on Cu_2O/G photocatalyst occurs mainly on the graphene component.

1. Introduction

In the context of decreasing atmospheric CO_2 emissions there is much current interest in developing efficient processes for the transformation of CO_2 into fuels and chemicals.[1, 2] One of the possibilities consists in developing photocatalytic CO_2 reductions.[3, 4] Among the various CO_2 reactions that can be considered, artificial photosynthesis in where CO_2 is reduced by action of a photocatalyst using solar light is one of the most appealing (Equation 1).[5, 6] However, due to the huge endothermicity of the process, the efficiency of most of the photocatalysts explored so far is very low, there being a need of more efficient materials.[7] In this context, it has been reported recently that Cu_2O nanoparticles on graphene (Cu_2O/G) is a very efficient photocatalyst for the overall water splitting [8] as well as for the photoassisted Sabatier methanation by H_2 of CO_2.[9]

$$CO_2 + 2H_2O \rightarrow CH_4 + 2O_2 \qquad \text{Eq. 1}$$

Continuing with this line of research it would be of interest to determine the efficiency of Cu_2O/G for CO_2 reduction in the presence of electron donors and to provide convincing evidence of the chemical electron reduction of CO_2 by the charge separated state of graphene-supported Cu_2O semiconductor. One general approach that has been widely used in photocatalytic H_2 generation by semiconductors has been to perform the reaction in the presence of electron donors as sacrificial agents (Scheme 1).[10] Under these conditions, after photoinduced charge separation into conduction band electrons and valence band holes, the later are readily scavenged by the electron donor and, therefore, the rate of H_2 evolution can be determined without limitation of the rate of h^+ consumption. In other words, while in photocatalysis oxidation by h^+ and reduction by e^- have to occur simultaneously, the presence of electron donors allow to study the photocatalytic reduction process without interference of the concomitant h^+ oxidation.

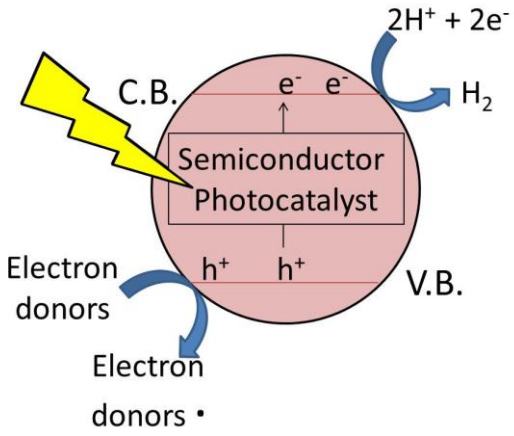

Scheme 1. Photocatalytic H_2 production upon photoinduced charge separation in semiconductor materials in the presence of a sacrificial electron donor.

Following this approach, i.e. performing photocatalytic CO_2 reduction by Cu_2O/G in the presence of electron donors, the present manuscript provides firm experimental evidence supporting that CO_2 can be photocatalytically reduced to

[a] Instituto Universitario de Tecnología Química CSIC-UPV, Universitat Politécnica de Valencia, Av. De los n s/n, 46022 Valencia. E-mail: hgarcia@gim.upv.es
[b] Center of Excellence in Advanced Materials Research, King Abdulaziz University, Jeddah, Saudi Arabia

Electronic Supplementary Information (ESI) available: [details of any supplementary information available should be included here]. See DOI: 10.1039/x0xx00000x

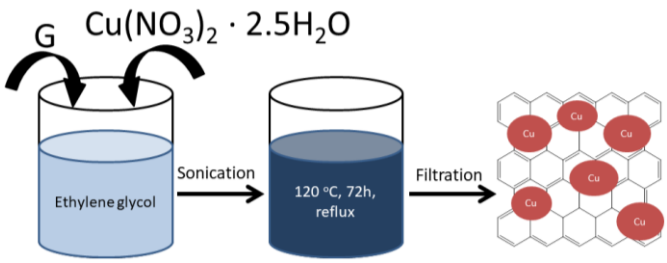

Scheme 2. Preparation of Cu_2O/G photocatalyst.

methane through a conventional photocatalytic mechanism involving charge separation state into e^- and h^+.

2. Experimental

2.1. Material preparation

Few-layers G (100 mg) dispersed in ethylene glycol (40 mL) was obtained from the pyrolysis under Ar flow at 900 ºC of alginic acid sodium salt from brown algae (Aldrich) and subsequent sonication in ethylene glycol at 750 W for 1 h, as reported before.[11] 7.3 mg of $Cu(NO_3)_2{\cdot}2.5H_2O$ were added to the suspension of G in ethylene glycol and chemical reduction was then performed at 120 ºC for 72 h under continuous stirring. The Cu_2O/G sample was finally separated from ethylene glycol by filtration and washed exhaustively with water and acetone. The resulting material was dried in a vacuum desiccator at 110 ºC to remove the remaining water.

2.2. Characterization

The amount of Cu present in the samples was determined by inductively coupled plasma-optical emission spectrometry (ICP-OES) by dissolving the Cu present in Cu_2O/G with *aqua regia* at room temperature for 3 h and analyzing the Cu content of the resulting solution.

Powder XRD patterns were recorded on a Shimadzu XRD-7000 diffractometer using Cu Kα radiation (λ = 1.5418 Å, 40 kV, 40 mA) at a scanning speed of 1 º per min in the 10-80 º 2 Theta range.

Raman spectra were collected with a Horiba Jobin Yvon-Labram HR UV-Visible-NIR (200-1.600 nm) Raman Microscope Spectrophotometer, using a 512 nm laser as excitation source. Raman spectra were obtained averaging 10 scans at a resolution of 2 cm^{-1}. HRTEM images were recorded in a JEOL JEM 2100F under 200 kV accelerating voltage. Samples were prepared by casting one drop of the suspended material in ethanol onto a carbon-coated copper TEM grid, and allowing it to dry at room temperature. XPS spectra were measured on a SPECS spectrometer equipped with a Phoibos 150 9MCD detector using a non-monochromatic X-ray source (Al and Mg) operating at 200 W. The samples were evacuated in a prechamber of the instrument at $1{\cdot}10^{-9}$ mbar. The binding energies of Cu 2p were corrected for surface charging by referring them to the binding energy of C 1s peak (284.5 eV). The measured intensity ratios of the components were obtained from the area of the corresponding peaks after nonlinear Shirley-type background subtraction and correction according to the response factor of each element in XPS. The equipment is calibrated using Cu, Ag and Au. Spectra deconvolution was made using the CasaXPS software.

2.3. Photocatalytic tests

A quartz photoreactor equipped with a nickel alloy thermocouple connected to a heating mantle and temperature controller was loaded with Cu_2O/G photocatalyst and located under the light spot. 20 µl of the electron donor was added with a microsyringe as a liquid onto the photocatalyst and CO_2 was introduced to achieve a final pressure of 1.3 bar. The equivalents of the different sacrificial electron donors are 1.5, 1.6, 1.7, 1.8 and 1.6 for triethanolamine (TEOA), dimethylaniline (DMA), thioanisole, anisole and *p*-xilene, respectively. Prior irradiation the photoreactor was heated at the desired temperature and when the desired temperature was stabilized the photocatalyst was irradiated from the top (2 cm above) through a fiber optics with UV-Vis light from a 300 W Xe lamp. Note that the time required before temperature equilibration can be about 30 min. The reaction products were analysed using an Agilent 490 MicroGC with two channels both of them with TC detectors and Ar as the carrier gas. One channel has a MolSieve 5A column and it analyses H_2 (temperature 62 ºC), among other light gases (N_2, O_2, CO). The second channel has a Pore PlotQ column and analyses CO_2 and up to C_4 hydrocarbons, among others gases (column temperature 75 ºC). No evidence of the formation of CH_3OH (detectable in the MicroGC equipment) was obtained. Quantification of the percentage of each gas was based on prior calibration of the system injecting mixtures with known percentage of gases.

3. Results and discussion

3.1. Photocatalyst characterization

The Cu_2O/G material used in the present study as photocatalyst was prepared following a procedure previously described in the literature.[8] In brief, the process consists in the polyol chemical reduction of Cu^{2+} at 120 ºC by ethylene glycol that contained defective graphene previously prepared by pyrolysis of alginic. In the process Cu^{2+} becomes reduced by ethylene glycol to Cu^+ and Cu^0 forming nanoparticles that become adsorbed on the graphene sheets. Scheme 2 illustrates the process of preparation of Cu_2O/G. As mentioned before, the G sample employed in the present preparation was obtained previously by pyrolysis of alginic acid sodium salt under Ar at 900 ºC and subsequent exfoliation of the turbostratic graphitic carbon residue by sonication in ethylene glycol.[12] This type of graphene has been fully characterized in the literature,[11, 13] and the present characterization data agree with the reported values. Chemical analysis indicates that G contains a residual amount of oxygen about 9 wt%. The presence of O_2 functional groups as well as carbon vacancies, formed in the pyrolytic process due to the evolution of CO_2 and CO, is responsible for the presence in the Raman spectrum of a D band at about 1350 cm^{-1}, accompanying the

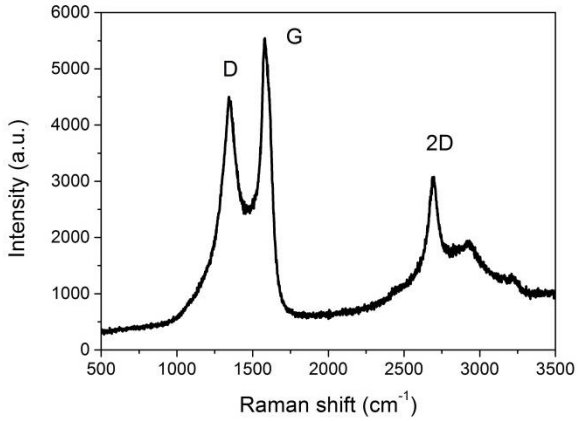

Figure 1. Raman spectrum from G obtained from alginic acid pyrolysis at 900 ºC under Ar atmosphere. Laser excitation at 512 nm.

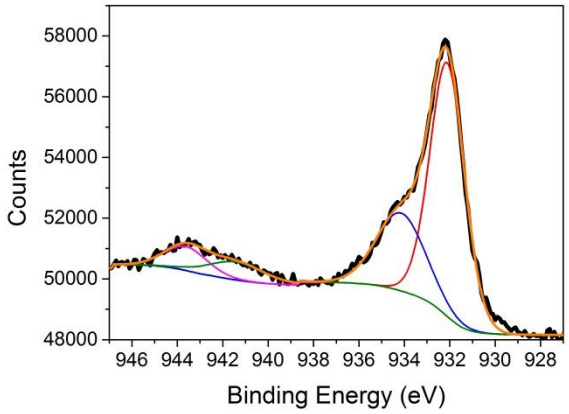

Figure 3. High resolution XPS peak for Cu 2p3/2 recorded for Cu_2O/G photocatalyst showing also its best deconvolution to individual components.

characteristic G peak at 1600 cm^{-1}. The ratio of the intensity of the G vs the D peak was 1.15 that is a quantitative indicator of the density of defects present on the G sheet. Figure 1 shows the Raman spectrum of the G sample used in the present study, where appearance of a sharp 2D peak at about 2700 cm^{-1}, indicative of the few layer configuration sample, is also observed.

XPS of G shows the corresponding C1s and O1s peaks. Deconvolution of experimental peaks shows that a percentage of about 80 % of carbon atoms corresponds to graphenic carbons appearing at a binding energy of 284.5 eV. The experimental C1s peak also shows other types of carbons associated to those C atoms bonded to oxygen with single and double bond at about 285.2 eV and carboxylic groups at 288.4 eV, with a relative proportion of 12 and 8 %, respectively (see Figure SI1 in Supplementary Information).

After exposure to the ambient atmosphere of the samples obtained from $Cu(NO_3)_2{\cdot}2.5H_2O$ polyol reduction in the presence of G, the presence of Cu_2O as predominant component is confirmed by XRD that shows the characteristics peaks expected for cubic phase of Cu_2O appearing at 2Θ values of 36, 42, 61 and 73 ^{0}.[9] Figure 2 shows the XRD pattern corresponding to the Cu_2O/G sample used in the present study.

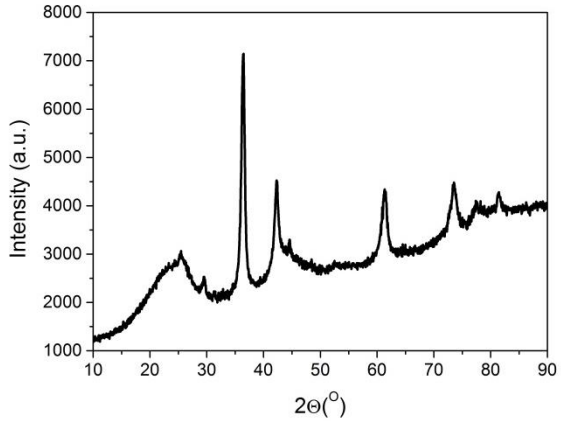

Figure 2. XRD pattern of the Cu_2O/G photocatalyst.

Importantly, XRD confirms that metallic Cu nanoparticles are absent or should correspond to a minor proportion of the total Cu present in the sample, since the characteristic peaks expected for cubic Cu metal nanoparticles are absent or very weak. Moreover, storage of Cu_2O/G exposed to the ambient for period of months does not alter the XRD pattern, showing that once obtained after the polyol Cu^{2+} reduction and fast formation of Cu_2O, no further oxidation takes place over a period of two months.

Figure 2 shows also a broad peak centred at 24^0 that is attributable to G powders constituted by loose packing of graphene sheets as previously reported.[14]

The average particle size of Cu_2O can be obtained from the width of the 111 peak by applying the Scherrer equation[15] resulting in an estimated average of 7.8 nm.

The Cu_2O content on the Cu_2O/G catalyst was determined by chemical analysis after dissolving all the Cu species in *aqua regia* and quantification of the resulting Cu^{2+} concentration by ICP-OES. It was determined that the Cu content was 1.74 wt% in the material.

The oxidation state of Cu_2O was also confirmed by XPS analysis of the Cu_2O/G by determining the binding energy and shape of the characteristic Cu $2p_{3/2}$ peak, Figure 3 shows the experimental XPS Cu $2p_{3/2}$ peak (-933 eV) and the accompanying satellite peaks (-943 eV) in good agreement with the values obtained in the literature,[8] together with the best fitting to possible individual components. Although XPS does not allow distinguishing between Cu^0 and Cu^{+1}, the corresponding Auger peak indicates that the major component of the $Cu2p_{3/2}$ was Cu^{+1} in agreement with the XRD pattern previously commented. In addition, deconvolution of the experimental $Cu2p_{3/2}$ peak also shows a contribution of about 40 % of Cu^{+2}. Since XPS is a surface technique and no CuO was observed by XRD, it is proposed that the minor Cu^{+2} should correspond to some CuO present on the outermost part of the Cu_2O particles.

The presence of Cu_2O nanoparticles on the G sheet was clearly observed by transmission electron microscopy. Figure 4 shows selected TEM images of the Cu_2O/G sample and the corresponding histogram of the particle size distribution. As it can be seen in the figures there is a relatively broad size

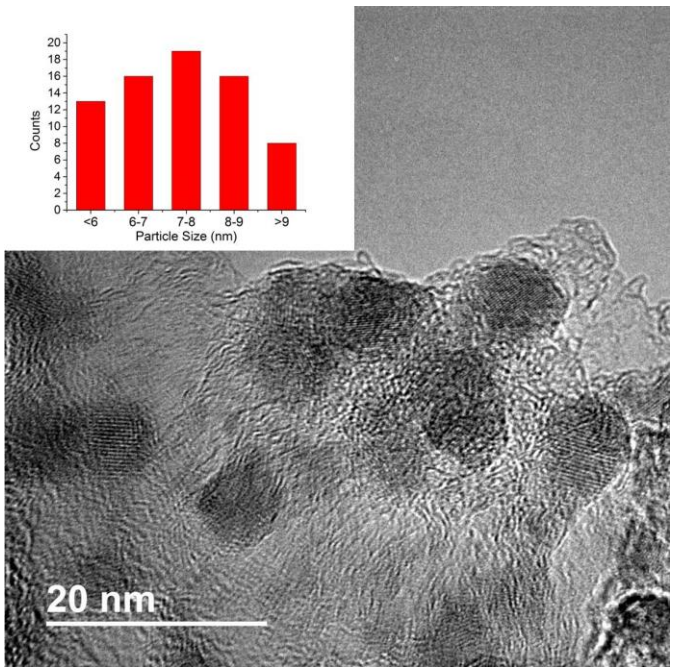

Figure 4. HRTEM image of Cu_2O/G. The inset shows size distribution histogram. Scale bar is 20 nm.

distribution of the particles with an average value about 7.6 ± 3.3 nm that is in relatively good agreement with the estimation based by XRD.

3.2. Photocatalytic tests

After preparation, Cu_2O/G was used as photocatalyst for the gas phase CO_2 reduction in the presence of sacrificial electron donors at temperatures about 200 °C. The only product observed in all cases was methane with almost complete selectivity. Particularly, CO and ethane, if formed, are in concentrations below the detection limit (<0.1%). Depending on the nature and redox potential of the sacrificial agent, the rate of methane production varied. Figure 5 shows a plot of the initial reaction rate of methane formation as a function of the redox potential of the electron donor. As it can be observed in this Figure an inverse relationship between the initial methane formation rate and the oxidation potential of electron donor was observed, the highest rate of methane formation, about 325 µmol $CH_4 \cdot g^{-1} \cdot h^{-1}$ being achieved for dimethylaniline (DMA), while the presence of poor electron donors alike *p*-xylene results in much lower CH_4 formation. A control experiment at 200 °C and 200 mW/cm² irradiation, but using G as photocatalyst, in the absence of Cu_2O NPs, has been carried out in the presence of DMA as electron donor for 2 h.
However, no detectable amounts of CH_4 were found. In a similar way, the photocatalytic CO_2 reduction was performed under dark conditions at 200 °C using Cu_2O as photocatalyst, but after 2 h reaction negligible CH_4, detectable but below the quantification limit, was found.

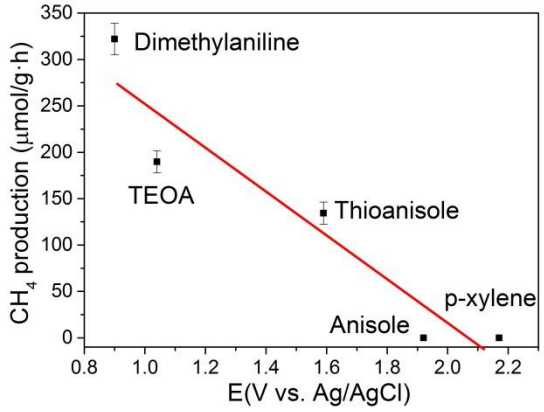

Figure 5. Initial CH_4 production rate as function of the sacrificial agent oxidation potential. The straight line shows the CH_4 production trend. The CH_4 production rate was measured under constant light intensity of 200 mW/cm² from a 300 W Xenon lamp at 200 °C. Reaction time was 1 h. 1.5, 1.6, 1.7, 1.8 and 1.6 equivalents of TEOA, DMA, thioanisole, anisole and *p*-xilene, respectively, were added to the reactor vessel in each experiment. TEOA = triethanolamine; DMA = dimethylaniline.

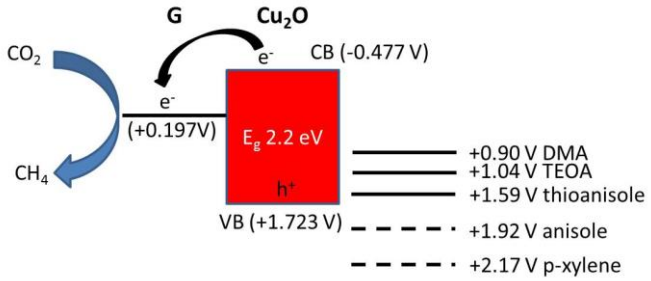

Scheme 3. Few layers graphene and Cu_2O band alignment, and oxidation potentials of the different electron donors vs. Ag/AgCl. TEOA = triethanolamine; DMA = dimethylaniline.

Overall the results presented in Figure 5 support a conventional photocatalytic mechanism for CO_2 reduction in where after charge separation induced by light absorption electrons and holes are generated. These electrons in the conduction band would be responsible for CO_2 reduction and CH_4 formation by multiple consecutive addition of eight electrons and eight protons. Concomitantly to the photogeneration of electrons consumed in the CO_2 reduction, holes will be generated. The role of the sacrificial electron donor is to quickly react with these holes forming protons. The formation of each CH_4 molecule will require the consumption of eight holes and the formation of eight protons. When H_2 is the reagent of the photothermal CO_2 reduction, this molecule is consuming holes and generating protons,[16] but sacrificial electron donors with lower oxidation potential will make the process faster.
The experimental results presented in Figure 5 and the previously commented photocatalytic mechanism are in good agreement with the reported energy values for the valence band maximum and conduction band minimum energies of Cu_2O semiconductor as well as the few layers G.[17, 18] As it presented in Scheme 3 the oxidation potentials of electron donors for which the rate of methane formation is above 100 µmol $CH_4 \cdot g^{-1} \cdot h^{-1}$, all have oxidation potentials smaller than

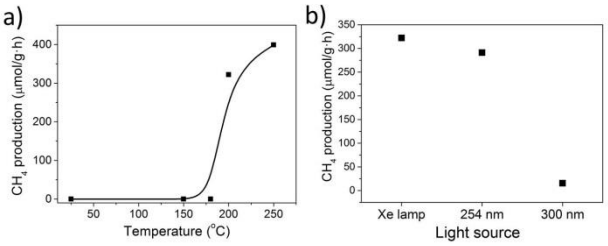

Figure 6. CH_4 production rate as function of temperature (a) and the used light filter (b) in the presence of dimethyl aniline. The CH_4 production rate was measured under constant light intensity of 200 mW/cm² from a 300 W Xenon lamp at 200 °C. Reaction time was 1h.

the valence band energy maximum and, therefore, electron from the sacrificial agent would readily quench holes on Cu_2O. Scheme 3 also shows that oxidation potentials of anisole and p-xylene are too high to allow these molecules to act as hole scavengers in Cu_2O and for this reason the rate of CH_4 production is much smaller.

On the other hand regarding the influence of the temperature of the photocatalytic process on the rate of methane production, a study of the photocatalytic CO_2 reduction in the presence of dimethylaniline at different temperatures was carried out and the results are presented in Figure 6a. It can be seen there that no CH_4 is formed at temperatures 177 °C or below, while the rate increases abruptly at temperatures above 180 °C. This drastic change in the CH_4 formation rate corresponds to the boiling temperature of dimethylaniline (T_b = 194 °C) and only when this sacrificial agent becomes in significant concentration in the gas phase can promote photocatalytic reduction of CO_2. Similar behaviour was observed for the other sacrificial agents, having boiling temperatures below the reaction temperature. It is worth noticing that although the boiling temperature of TEOA is 335 °C, the small amount (20 μL) added in the reaction vessel at 200 °C seems be enough to produce sufficient TEOA vapor pressure, promoting the photocatalytic reduction of CO_2. The presence of vapors of sacrificial electron donors in contact with the photocatalyst ensures fast diffusion and quenching of the photogenerated holes.

The spectral response of Cu_2O/G for CO_2 reduction was studied by using the full output of a Xe lamp emitting from 250 nm in the whole range of UV and visible wavelengths and by filtering this polychromatic light with cut-off filters. The results are presented in Figure 6b. As it can be seen there, the photoresponse of Cu_2O/G derives mainly from the UV light below 300 nm, since methane production rate becomes very small for wavelength longer than this UV wavelength. These results suggest that the photons responsible for the CO_2 reduction are mainly those absorbed by the few layers defective graphene and the Cu_2O NPs in the UV region. After light absorption electron transfer between graphene and Cu_2O should occurs with electrons located on the graphene sheet and holes on the Cu_2O. There is a large number of precedents in the literature in where the positive influence of graphene enhancing the photocatalytic activity of semiconductors has been also observed and attributed to the electro transfer from the semiconductor to graphene, resulting in electron

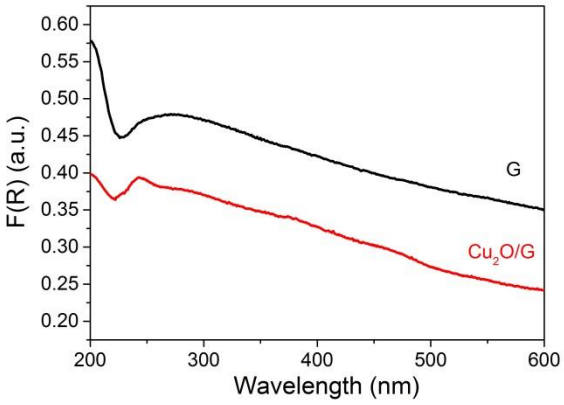

Figure 7. Diffuse reflectance UV-Vis spectra, plotted as the Kubelka-Munk function of the reflectance F(R), of G (black) and Cu_2O/G (red).

delocalisation on the graphene sheet and holes located on the semiconductor.[19] A similar proposal would apply here, as can be observed in Scheme 3. Optical absorption spectrum of G and Cu_2O/G are characterized by absorption bands at λ_{max} 276 and 248 nm, respectively, in agreement with this rationalization, since the UV absorption band is present both in G and Cu_2O/G, as can be observed in Figure 7.

It is possible that the low proportion of Cu_2O/G photocatalyst is responsible for the low visible light absorption observed in the spectrum of Cu_2O/G that is remarkably similar to that of G, although a small blue shift in the UV-Vis spectra can be observed when Cu_2O are supported in G. Also the photocatalytic behaviour of defective graphene acting as semiconductor has been already reported in the literature.[20]

Conclusions

The present results show that there is an inverse relationship between the oxidation potential of sacrificial agents as electron donors and the initial methane production rate using Cu_2O/G as photocatalyst. This relationship is indicative that the mechanism of the photocatalytic CO_2 reduction should involve photoinduced charge separation with the generation of electrons and holes. In this way those molecules whose oxidation potential is higher than the valence band energy maximum of the Cu_2O are not efficient for the generation of methane. On the contrary, the initial rate of CH_4 production increases as the oxidation potential of the electron donor decreases in an almost linear relationship. These results open the way for a more efficient photocatalytic CO_2 reduction using photocatalysts based on graphene and serve to rationalize the mechanism of related photoassisted CO_2 reduction by hydrogen (Sabatier photomethanation) that could also occur on Cu_2O/G through photogenerated charge separated states rather than a photothermal mechanism in which the energy of light is thermalized and converted into heat.

Conflicts of interest

There are no conflicts to declare.

Acknowledgements

Financial support by the Spanish Ministry of Economy and Competitiveness (Severo Ochoa, GRAPAS, and CTQ2015-69563-CO2-R1) and by the Generalitat Valenciana (Prometeo 2015-083) is gratefully acknowledged. J. A. thanks the Universitat Politècnica de València for a postdoctoral scholarship. D. M. also thanks Spanish Ministry of Science for PhD Scholarship.

Notes and references

1. J. Wei, Q. Ge, R. Yao, Z. Wen, C. Fang, L. Guo, H. Xu and J. Sun, *Nature Communications*, 2017, **8**, 15174.
2. O. Ola, M. Mercedes Maroto-Valer and S. Mackintosh, *Energy Procedia*, 2013, **37**, 6704-6709.
3. C. Peng, G. Reid, H. Wang and P. Hu, *The Journal of Chemical Physics*, 2017, **147**, 030901.
4. G. Zhao, X. Huang, X. Wang and X. Wang, *Journal of Materials Chemistry A*, 2017, **5**, 21625-21649.
5. F. E. Osterloh, *ACS Energy Letters*, 2017, **2**, 445-453.
6. N. S. Lewis, *Nature Nanotechnology*, 2016, **11**, 1010.
7. Q. Xu and T. Kobayashi, *Advanced Materials for Clean Energy*, Boca Raton: CRC Press, 2015.
8. D. Mateo, I. Esteve-Adell, J. Albero, A. Primo and H. García, *Applied Catalysis B: Environmental*, 2017, **201**, 582-590.
9. D. Mateo, J. Albero and H. Garcia, *Energy & Environmental Science*, 2017.
10. Z. Han and R. Eisenberg, *Accounts of Chemical Research*, 2014, **47**, 2537-2544.
11. C. Lavorato, A. Primo, R. Molinari and H. García, *ACS Catalysis*, 2014, **4**, 497-504.
12. M.-M. Trandafir, M. Florea, F. Neaţu, A. Primo, V. I. Parvulescu and H. García, *ChemSusChem*, 2016, **9**, 1565-1569.
13. A. Primo, F. Neatu, M. Florea, V. Parvulescu and H. Garcia, *Nature Communications*, 2014, **5**, 5291.
14. S. Liu, M.-Q. Yang, N. Zhang and Y.-J. Xu, *Journal of Energy Chemistry*, 2014, **23**, 145-155.
15. A. L. Patterson, *Physical Review*, 1939, **56**, 978-982.
16. E. Karamian and S. Sharifnia, *Journal of CO2 Utilization*, 2016, **16**, 194-203.
17. Y. Xu and M. A. A. Schoonen, *American Mineralogist*, 2000, **85**, 543-556.
18. O. Leenaerts, B. Partoens, F. M. Peeters, A. Volodin and C. V. Haesendonck, *Journal of Physics: Condensed Matter*, 2017, **29**, 035003.
19. J. Ran, J. Zhang, J. Yu, M. Jaroniec and S. Z. Qiao, *Chemical Society Reviews*, 2014, **43**, 7787-7812.
20. C. Lavorato, A. Primo, R. Molinari and H. Garcia, *Chemistry – A European Journal*, 2014, **20**, 187-194.

